Journal of Solid State Chemistry 221 (2015) 306–310

Contents lists available at ScienceDirect

Journal of Solid State Chemistry

journal homepage: www.elsevier.com/locate/jssc

Single crystal and magnetic structures of maricite-type $AgMnVO_4$

Hamdi Ben Yahia [a,*], Masahiro Shikano [a,*], Etienne Gaudin [b], Maxim Avdeev [c], Chris D. Ling [d]

[a] *Research Institute for Ubiquitous Energy Devices, National Institute of Advanced Industrial Science and Technology (AIST), 1-8-31, Midorigaoka, Ikeda, Osaka 563-8577, Japan*
[b] *ICMCB, CNRS, Université Bordeaux 1, 87 Avenue du Docteur Schweitzer, 33608 Pessac Cedex, France*
[c] *Bragg Institute, Australian Nuclear Science and Technology Organisation, Lucas Heights, NSW 2234, Australia*
[d] *School of Chemistry, The University of Sydney, Sydney, NSW 2006, Australia*

ARTICLE INFO

Article history:
Received 19 August 2014
Received in revised form
15 September 2014
Accepted 18 September 2014

Keywords:
Vanadate
Flux growth
Single crystal
Magnetic structure

ABSTRACT

Single crystals of the ternary manganese vanadate $AgMnVO_4$, were grown using $AgVO_3$ flux. The structure was determined from single crystal X-ray diffraction data. The magnetic structure and properties of $AgMnVO_4$ were characterized by magnetic susceptibility, specific heat, and low-temperature neutron powder diffraction measurements. $AgMnVO_4$ crystallizes in the maricite-type structure with space group *Pnma*, $a=9.5393(12)$, $b=6.8132(9)$, $c=5.3315(7)$ Å and $Z=4$. $AgMnVO_4$ contains MnO_4 chains made up of edge-sharing MnO_6 octahedra, and these chains are interlinked by the VO_4 and AgO_4 tetrahedra. The specific heat measurements indicate a 3D-antiferromagnetic ordering at ~12.1 K and the neutron powder diffraction measurements at 5 K show that the Mn^{2+} magnetic moments are antiferromagnetically coupled within the chains which are antiferromagnetically coupled to each other.

1. Introduction

Phosphates with the general formula $ABPO_4$ (A = K, Rb and Cs; B = transition metal) crystallize mainly in two different structural types, i.e., stuffed-tridymite and zeolite-ABW. Members of these families are characterized by a BPO_4^- tetrahedral framework, which can show four-, six-, or eight membered rings. Sometimes, the transition metal is found at a trigonal bipyramidal site. In the more condensed phases $ABPO_4$ (A = Li, Na; B = transition metal) with olivine and maricite-type structures, the transition metal is located at octahedral sites.

It is of interest to compare the structural evolution between homologous phosphates and vanadates, $AMnPO_4$ and $AMnVO_4$, respectively. In the $AMnPO_4$ phosphates series, $LiMnPO_4$ [1] $NaMnPO_4$ [2] $KMnPO_4$ [3] and $CsMnPO_4$ [4] have been studied and their structures determined. Recently, we reported the structural and magnetic properties of $RbMnPO_4$ [5,6] and $AgMnPO_4$ [7]. In the homologous $AMnVO_4$ vanadates, $LiMnVO_4$ [8] is known to crystallize in the Na_2CrO_4-type structure. Recently, the $AMnVO_4$ vanadate series has been extended by the addition of $AgMnVO_4$ [9], $CuMnVO_4$ [10], $NaMnVO_4$ [11], $KMnVO_4$ [12], and $RbMnVO_4$ [9]. $AgMnVO_4$ and $NaMnVO_4$ crystallize in the maricite-type structure and contains MnO_4 chains made up of edge-sharing MnO_6 octahedra. $CuMnVO_4$ crystallizes in the Na_2CrO_4-type structure and also contains MnO_4 chains made up of edge-sharing MnO_6 octahedra. Surprisingly, $KMnVO_4$ crystallizes in a new type of oxygen-deficient perovskite, and $RbMnVO_4$ is the first vanadate crystallizing in the stuffed tridymite-type structure [9].

All the crystal structures of the $AMnVO_4$ vanadate series have been solved from single crystal data, except $AgMnVO_4$. Its structure had so far only been characterized on the basis of powder X-ray diffraction data, since this compound has an incongruent melting point and decomposes above 750 °C [9]. Herein we report on crystal growth studies and a precise single crystal structure refinement for $AgMnVO_4$. Furthermore, we have solved the magnetic structure from low temperature neutron powder diffraction (NPD) data. Results of our studies are described in the following.

2. Experimental

2.1. Synthesis

$AgMnVO_4$ was prepared by solid state reaction from a stoichiometric mixture of Ag_2O, MnO and V_2O_5 powders as previously reported [9]. $AgMnVO_4$ was then mixed with an excess of an equimolar amount of Ag_2O and V_2O_5, pelletized, and fired at 700 °C for 8 h under argon flow. During this step Ag_2O reacts with

---

[*] Corresponding authors. Tel.: +81 72 751 7932; fax: +81 72 751 9609.
E-mail addresses: benyahia.hamdi@voila.fr (H. Ben Yahia), shikano.masahiro@aist.go.jp (M. Shikano).

http://dx.doi.org/10.1016/j.jssc.2014.09.017
0022-4596/

V_2O_5 forming $AgVO_3$ which melts at 476 °C [13] and therefore plays the role of flux for the crystal growth of $AgMnVO_4$. By a relatively fast decrease of the temperature, at the rate of 15 °C h^{-1} to room temperature, red, black, and white single crystals were obtained. They have been identified, using EDX and single crystal diffraction analyses, as $AgMnVO_4$, $Mn_2V_2O_7$, and $AgVO_3$, respectively.

2.2. Electron microprobe analysis

Semiquantitative EDX analyses of different single crystals including the ones investigated on the diffractometer were carried out with a JSM-500LV (JEOL) scanning electron microscope (SEM). The experimentally observed compositions were close to the ideal one $AgMnVO_4$ (Fig. 1). Some crystals showed compositions close to $Mn_2V_2O_7$ and $AgVO_3$.

2.3. Single crystal X-ray diffraction measurements

$AgMnVO_4$ single crystals suitable for single crystal X-ray diffraction were selected on the basis of the size and the sharpness of the diffraction spots. The data collections were carried out on a Smart Apex diffractometer using Mo$K\alpha$ radiation. Data processing and all refinements were performed with the Jana 2006 program package [14]. A Gaussian-type absorption correction was applied, and the shape was determined with the video microscope of the diffractometer. For the $AgMnVO_4$ data collection details, see Table 1.

2.4. Magnetic susceptibility and specific heat capacity measurements

DC magnetic susceptibility data for $AgMnVO_4$ were collected in the zero field cooled (ZFC) and field cooled (FC) modes on a Physical Property Measurement System (PPMS, Quantum Designs) in magnetic field of 5 kOe over the temperature range of 2–300 K. Isothermal magnetization was measured in the field of up to 10 kOe. Heat capacity measurements were performed on $AgMnVO_4$ pellet using a PPMS Quantum Design in a temperature range from 4 to 30 K.

2.5. Neutron powder diffraction

NPD data were collected on the high-resolution diffractometer Echidna at the OPAL facility (Lucas Height, Australia) using neutrons of wavelength 2.4395 Å. For the measurements the sample in the form of ~1 g of powder was loaded in a 6 mm diameter cylindrical vanadium can and the data were collected at 5 and 30 K using a closed-cycle refrigerator. The Rietveld analysis of the data was performed using the Fullprof Suite with the default neutron scattering lengths and Mn^{2+} magnetic form-factors.

3. Results and discussion

3.1. Structure refinement

The extinction conditions observed for single crystal $AgMnVO_4$ agree with the *Pnma* and $Pn2_1a$ space groups. The refinement was performed taking into account the centrosymmetric space group

Table 1
Crystallographic data and structure refinement for $AgMnVO_4$.

Chemical formula	$AgMnVO_4$
Crystal color	Red
Crystal size mm	0.100 × 0.090 × 0.045
M (g mol^{-1})	277.7
Crystal system	Orthorhombic
Space group	*Pnma*
a (Å)	9.5393(12)
b (Å)	6.8132(9)
c (Å)	5.3315(7)
V ($Å^3$)	346.51(8)
Z	4
Density calcd. (g cm^{-3})	5.32
Temperature (K)	293(1)
F(0 0 0) (e)	508
Diffractometer	SMART APEX
Monochromator	Graphite
Radiation (Å)	Mo$K\alpha$, 0.71069
Scan mode	Multi-scan
$h\ k\ l$ range	± 12, $-8 \le k \le 7$, $-7 \le l \le 6$
θ_{min}, θ_{max} (°)	4.27, 28
Linear absorption coeff. (mm^{-1})	11.67
Absorption correction	Gaussian
T_{min}/T_{max}	0.3573/0.6248
No. of reflections	2304
No. of independent reflections	387
Reflections used [$I \ge 0\sigma(I)$]	387
R_{int}	0.024
Refinement	F^2
No. of refined parameters	41
R factors $R(F)/wR(F^2)$	0.0307/0.0790
g. o. f.	1.33
Weighting scheme	$w=1/(\sigma^2(I)+0.0016I^2)$
Diff. Fourier residues (e^- $Å^{-3}$)	−0.82/+0.61

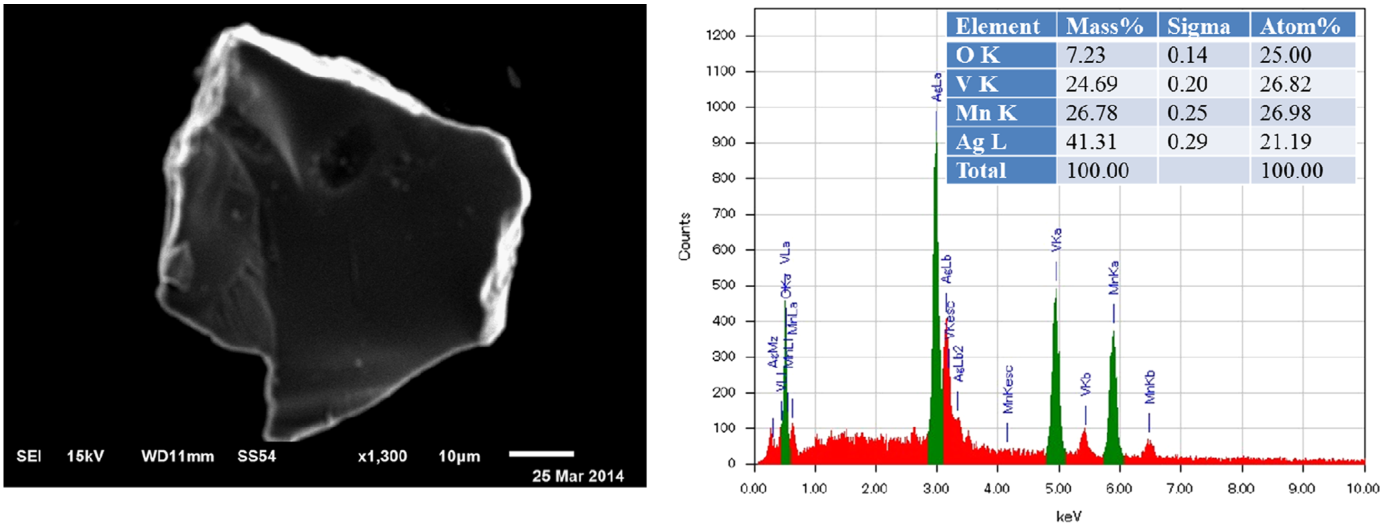

Element	Mass%	Sigma	Atom%
O K	7.23	0.14	25.00
V K	24.69	0.20	26.82
Mn K	26.78	0.25	26.98
Ag L	41.31	0.29	21.19
Total	100.00		100.00

Fig. 1. Image and EDX analyses of the $AgMnVO_4$ single crystal used for the data collection.

Pnma. Most of the atomic positions were found by superflip program implemented in Jana 2006 program package. With anisotropic atomic displacement parameters, the final residual factors converged to the value $R(F)=0.0307$ and $wR(F^2)=0.0790$ for 41 refined parameters, 387 independent reflections and difference-Fourier residues in the range between -0.82 and $+0.61\ e\ Å^{-3}$. The refined atomic positions and anisotropic displacement parameters (ADPs) are given in Tables 2 and 3, respectively.

3.2. Crystal structure of $AgMnVO_4$

$AgMnVO_4$ is isostructural with maricite-type $NaMnPO_4$. The structure consists of edge-sharing chains of MnO_6 octahedra running along the *b* axis. The MnO_6 octahedra are cross-connected by the VO_4 and AgO_4 tetrahedra (Fig. 2). No significant differences were observed compared to the structure solved from powder diffraction data [9]. The interatomic distances and the bond valence sums (BVS) [15,16] are given in Table 4.

The Mn–O distances range from 2.099 to 2.342 Å with a mean distance of 2.202 Å. This is very similar to the results found for $NaMnPO_4$ and $NaMnVO_4$, in which the Mn–O distances range from 2.077 to 2.397 Å and from 2.099 to 2.368 Å with mean distances of 2.229 and 2.216 Å, respectively. The BVS of 2.042 is in good agreement with the expected value of +2 for high-spin $Mn^{2+}(d^5)$ [17].

The vanadium tetrahedra are quite regular with distances ranging from 1.678 to 1.767 Å and a mean value of 1.716 Å. The O–V–O angles range from 105.82(13)° to 115.68(19)° with a mean value of 109.39°. The BVS of 5.085 is in agreement with the expected value of +5 for V^{5+}.

The Ag^+ ion is bonded to four O atoms belonging to four different MnO_6 groups to form an irregular tetrahedron. The Ag–O distances range from 2.293 Å to 2.479 Å with a mean value of 2.351 Å. The O–Ag–O angles range from 86.32(7)° to 128.84(9)° with a mean value of 108.21°. The BVS is calculated to be 1.031 for the four-coordinate silver atom.

3.3. Magnetic susceptibility and specific heat measurements of $AgMnVO_4$

Based on the previously reported magnetic property measurements, a long-range antiferromagnetic (AFM) ordering transition was expected at 12.3 K [9]. Our magnetic susceptibility data also revealed the presence of a neglectable amount of Mn_3O_4 which orders ferromagnetically below 43 K (Fig. S1) [18]. The field used for the measurements was apparently sufficiently high to suppress its contribution as analysis of the data in the range above 200 K with the Curie–Weiss law yielded the results in close agreement with those previously reported: $\mu_{eff} = 5.74\,\mu_B$ and $\theta = -55$ K compared to $5.96\,\mu_B$ and $\theta = -62$ K [9]. In addition, our heat capacity data showed a clear lambda-type (Fig. S1, inset) anomaly at 12.1 K signalling a long-range magnetic ordering transition in excellent agreement with the previously reported measurements [9].

Table 2
Fractional atomic coordinates and isotopic atomic displacement parameters (Å^2) for $AgMnVO_4$.

Atom	Wyck.	Symm.	*x*	*y*	*z*	U_{eq} (Å^2)
Ag	4*c*	*.m.*	0.35033(7)	1/4	0.00305(7)	0.0208(2)
Mn	4*a*	−1	1/2	1/2	1/2	0.0106(3)
V	4*c*	*.m.*	0.67960(11)	1/4	0.02069(14)	0.0050(3)
O1	4*c*	*.m.*	0.8636(4)	1/4	0.0587(8)	0.0096(10)
O2	4*c*	*.m.*	0.6198(4)	1/4	−0.2881(6)	0.0106(10)
O3	8*d*	1	0.6159(3)	0.4465(4)	0.1725(5)	0.0121(7)

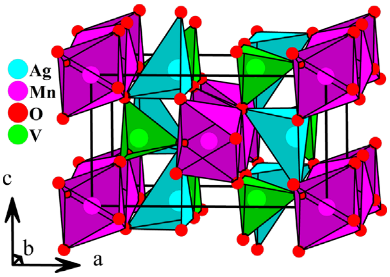

Fig. 2. Projection view of the structure of $AgMnVO_4$.

Table 4
Interatomic distances (in Å) and corresponding bond valences (BV) for $AgMnVO_4$. Mean distances are given in brackets.

	distance	BV
Ag–O3 (× 2)	2.293(3)	0.296
Ag–O1	2.340(4)	0.260
Ag–O2	2.479(4)	0.179
	⟨2.351⟩	1.031[a]
Mn–O3 (× 2)	2.099(2)	0.434
Mn–O1 (× 2)	2.166(2)	0.362
Mn–O2 (× 2)	2.342(2)	0.225
	⟨2.202⟩	2.042[a]
V–O1	1.767(4)	1.102
V–O2	1.742(4)	1.179
V–O3 (× 2)	1.678(3)	1.402
	⟨1.716⟩	5.085[a]
O3–V–O3	105.82(13)	
O1–V–O3 (× 2)	107.70(12)	
O2–V–O3 (× 2)	109.73(11)	
O1–V–O2	115.68(19)	
	⟨109.39⟩	
O2–Ag–O3 (× 2)	86.32(7)	
O1–Ag–O3 (× × 2)	113.58(6)	
O1–Ag–O2	120.63(12)	
O3–Ag–O3	128.84(9)	
	⟨108.21⟩	

[a] Bond valence, $BV=\exp\{(r_0-r)/b\}$ with the following parameters: $b=0.37$, r_0 (Ag^I–O) = 1.843, r_0 (Mn^{II}–O) = 1.790 and r_0 (V^V–O) = 1.803 Å [15,16].

Table 3
Anisotropic atomic displacement parameters (Å^2) for $AgMnVO_4$. The anisotropic displacement factor exponent takes the form: $-2\pi^2[(ha^*)^2U_{11}+\dots+2hka^*b^*U_{12}]$.

Atom	U_{11}	U_{22}	U_{33}	U_{12}	U_{13}	U_{23}
Ag	0.0245(5)	0.0223(4)	0.0156(4)	0	−0.00118(14)	0
Mn	0.0095(5)	0.0126(6)	0.0097(6)	−0.0041(3)	0.0049(2)	−0.0034(2)
V	0.0040(5)	0.0058(5)	0.0051(5)	0	0.0009(3)	0
O1	0.0037(19)	0.0099(18)	0.0151(16)	0	0.0015(14)	0
O2	0.0125(19)	0.0130(18)	0.0063(16)	0	−0.0006(13)	0
O3	0.0115(13)	0.0130(12)	0.0116(12)	0.0030(10)	0.0038(9)	−0.0017(9)

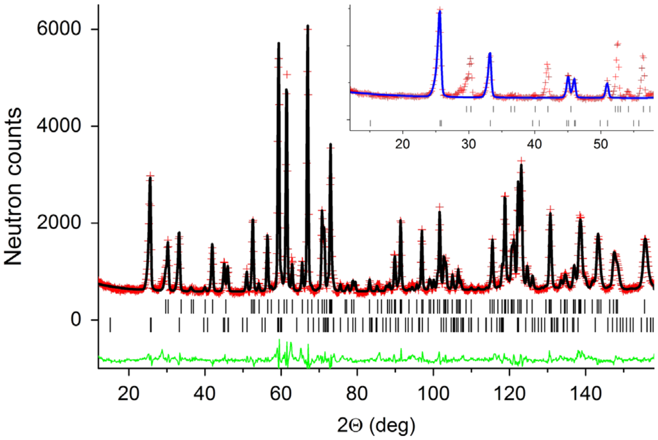

Fig. 3. The Rietveld plot for $AgMnVO_4$ refined against NPD data collected at 5 K. The red crosses and black and green solid lines indicate the observed and calculated patterns and their difference, respectively. The tick marks from top to bottom indicate the position of the diffraction peaks of the nuclear and magnetic structure, respectively. $R_p = 4.23\%$, $R_{wp} = 5.58\%$, $\chi^2 = 2.34$, $R_{mag} = 9.24\%$. The blue curve in the inset shows the magnetic contribution only. (For interpretation of the references to color in this figure legend, the reader is referred to the web version of this article.)

3.4. *Crystal and magnetic structure from neutron powder diffraction measurements*

NPD data collected for $AgMnVO_4$ at 30 K (i.e., above the transition expected based on our heat capacity measurements) were successfully analysed using the structure model determined from the X-ray single crystal diffraction data. Since NPD is unable to precisely determine vanadium atom positions due to its very low scattering length, the coordinates were fixed to those from Table 2. The final Rietveld fit and crystallographic information for $AgMnVO_4$ at 30 K are presented in Fig. S2 and Table S1, respectively.

Examination of the NPD data collected at 5 K revealed additional intensity due to long-range magnetic ordering (Fig. 3). All the diffraction peaks with magnetic contributions could be indexed to a unit cell with doubled *a*- and *c*-parameters, i.e., with the propagation vector $k = (1/2, 0, 1/2)$. Few additional peaks of negligible intensity were identified as those of Mn_3O_4, which is consistent with both susceptibility and field dependent magnetization data (Fig. S1) as Mn_3O_4 ferrimagnetically orders below 43 K [18]. Results of representational analysis for the 4*a* (0, 0, 0) Wyckoff site of the *Pnma* space group with such a propagation vector were previously reported in Ref. [19]. Although by symmetry the four manganese sites split into two pairs, which are allowed to carry different magnetic moments, we assumed equal moment values on all Mn atoms. The best agreement between experimental and calculated NPD patterns was obtained for the combination of $\Gamma1+\Gamma5$ irreducible representations [19]. Examination of the data showed no evidence for scattering due to a magnetic moment component along the *b*-axis, therefore, only the parameters defining the moment in the *ac*-plane were refined. The final Rietveld plot and crystallographic information are presented in Fig. 3 and Table S2. The resulting magnetic structure, which can also be described by the $P_{2a}2_1/m$ group (Opechowski-Guccione #11.6.64) is illustrated in Fig. 4. The components of the magnetic moment along the *a*- and *c*-axes are 2.73(8) and 2.93(8) μ_B, respectively, yielding the total moment of 4.01(8) μ_B. The moment value reduction compared to the theoretical value of 5 μ_B for high-spin d^5 ($S = 5/2$) Mn^{2+} is likely due to the quasi-one-dimensional magnetic topology of $AgMnVO_4$ (Fig. 4) in which exchange along the edge-sharing octahedral chains can be easily disrupted by local chemical disorder.

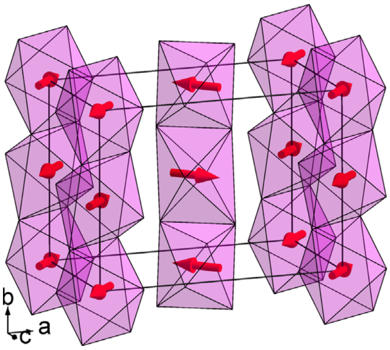

Fig. 4. General view of the crystal and magnetic structure of $AgMnVO_4$.

Examination of the magnetic structure reveals that the orientation of Mn^{2+} magnetic moments is almost identical to that of Fe^{2+} in isostructural maricite-type $NaFePO_4$ [19]. However, while in $NaFePO_4$ the edge-sharing octahedral chains are ferromagnetic, in $AgMnVO_4$ they are antiferromagnetic. This is not surprising as in contrast to d^6–d^6 interactions of Fe^{2+} in $NaFePO_4$, in case of $AgMnVO_4$ weak d^5–d^5 antiferromagnetic coupling is promoted by both “90° superexchange” *via* shared oxygen atoms and direct cation–cation exchange between half-filled t_{2g} orbitals of Mn^{2+} [20,21].

4. Concluding remarks

The crystal structure of $AgMnVO_4$ was determined using single crystal X-ray diffraction data for the first time. In agreement with previous results based on powder diffraction data, the structure was found to crystallize with the maricite type. Low-temperature physical property measurements and neutron powder diffraction experiments showed that the compound undergoes long-range antiferromagnetic ordering transition at 12.1 K. Although $AgMnVO_4$ and $NaFePO_4$ crystallize in the maricite-type structure, the magnetic structures of the two compounds are significantly different in that the spins are antiferromagnetically- and ferromagnetically-coupled within the chains of $AgMnVO_4$ and $NaFePO_4$, respectively. This difference is explained by the combined effect of oxygen mediated 90°-superexchange and direct d^5–d^5 cation–cation exchange in the former in contrast to d^6–d^6 interactions in the latter.

Acknowledgments

Part of this work was supported by Grant-in-Aid for the Japan Society for the Promotion of Science (JSPS) Fellows Grant number 24●02506.

Appendix A. Supporting information

Supplementary data associated with this article can be found in the online version at http://dx.doi.org/10.1016/j.jssc.2014.09.017.

References

[1] S. Geller, J.L. Durand, Acta Crystallogr 13 (1960) 325–331.
[2] J. Moring, E. Kostiner, J. Solid State Chem. 61 (1986) 379–383.
[3] M. Lujan, F. Kubel, H. Schmid, Z. Naturforsch. 50b (1995) 1210–1214.
[4] O.V. Yakubovich, M.A. Simonov, O.K. Mel'nikov, Kristallografiya 35 (1990) 42–46.
[5] H. Ben Yahia, E. Gaudin, J. Darriet, J. Alloys Compd 442 (2007) 74–76.
[6] G. Nénert, J. Lamont Bettis, R. Kreimer, H. Ben Yahia, C. Ritter, E. Gaudin, O. Isnard, M.H. Whangbo, Inorg. Chem 52 (2013) 9627–9635.
[7] H. Ben Yahia, E. Gaudin, J. Darriet, Z. Naturforsch 64b (2009) 875–878.

[8] A.K. Padhi, W.B. Archibald, K.S. Nanjundaswamy, J.B. Goodenough, Solid State Chem 128 (1997) 267–272.
[9] H. Ben Yahia, E. Gaudin, J. Darriet, J. Solid State Chem. 181 (2008) 3103–3109.
[10] H. Ben Yahia, E. Gaudin, J. Darriet, M. Banks, R.K. Kremer, A. Villesuzanne, M.H. Whangbo, Inorg. Chem. 44 (2005) 3087–3093.
[11] H. Ben Yahia, E. Gaudin, K. Boulahya, J. Darriet, Inorg. Chem. 49 (2010) 8578–8582.
[12] H. Ben Yahia, E. Gaudin, C. Lee, M.H. Whangbo, J. Darriet, Chem. Mater. 19 (2007) 5563–5569.
[13] S. Kittaka, K. Matsuno, H. Akashi, J. Solid State Chem. 142 (1999) 360–367.
[14] V. Petricek, M. Dusek, L. Palatinus, Z. Kristallogr. 229 (2014) 345–352.
[15] I.D. Brown, D. Altermatt, Acta Crystallogr B41 (1985) 244–247.
[16] N.E. Brese, M. O'Keefe, Acta Crystallogr B47 (1991) 192–197.
[17] R.D. Shannon, Acta Crystallogr A32 (1976) 751–767.
[18] B. Chardon, F. Vigneron, J. Magn. Magn. Mater. 58 (1986) 128–134.
[19] M. Avdeev, Z. Mohamed, C.D. Ling, J. Lu, M. Tamaru, A. Yamada, P. Barpanda, Inorg. Chem. 52 (2013) 8685–8693.
[20] K. Motida, S. Miyahara, J. Phys. Soc. Japan 28 (1970) 1188–1196.
[21] J.B. Goodenough, Phys. Rev. 117 (1960) 1442–1451.